INTERNATIONAL JOURNAL FOR NUMERICAL METHODS IN FLUIDS, VOL. 13, 355–369 (1991)

A BOUNDARY INTEGRAL EQUATION METHOD FOR NAVIER–STOKES EQUATIONS—APPLICATION TO FLOW IN ANNULUS OF ECCENTRIC CYLINDERS

P. S. RAMESH

Xerox Corporation, Design Research Institute, Engineering and Theory Center, Cornell University, Ithaca, NY 14853, U.S.A.

AND

M. H. LEAN

Xerox Corporation, Webster Research Center, Mechanical Engineering Sciences Laboratory, North Tarrytown, NY 10591, U.S.A.

SUMMARY

A novel Navier–Stokes solver based on the boundary integral equation method is presented. The solver can be used to obtain flow solutions in arbitrary 2D geometries with modest computational effort. The vorticity transport equation is modelled as a modified Helmholtz equation with the wave number dependent on the flow Reynolds number. The non-linear inertial terms partly manifest themselves as volume vorticity sources which are computed iteratively by tracking flow trajectories. The integral equation representations of the Helmholtz equation for vorticity and Poisson equation for streamfunction are solved directly for the unknown vorticity boundary conditions. Rapid computation of the flow and vorticity field in the volume at each iteration level is achieved by precomputing the influence coefficient matrices. The pressure field can be extracted from the converged streamfunction and vorticity fields. The solver is validated by considering flow in a converging channel (Hamel flow). The solver is then applied to flow in the annulus of eccentric cylinders. Results are presented for various Reynolds numbers and compared with the literature.

KEY WORDS Boundary integral equation method Navier–Stokes equation Method of characteristics Hamel flow Eccentric cylinder annulus Rotating cylinders

1. INTRODUCTION

The value of computer analysis is now widely recognized by the industrial community. Because of this, there is considerable interest in developing generalized numerical algorithms which are more flexible and efficient than conventional finite difference and finite element methods. These algorithms must handle realistic physical situations involving complex geometries and strong non-linear couplings between fluid dynamics, electrostatics, electromagnetics, heat transfer, etc. Boundary integral equation methods are being proposed as a possible alternative to domain methods. This paper describes the solution of Navier–Stokes equations in the annulus of eccentric cylinders using boundary integral equation methods.

In the past, boundary integral equation methods (BIEM) have been used extensively to solve potential flow problems.[1] Kelmanson[2] used BIEM to study Stokes flow in the annulus of eccentric cylinders. Recently some researchers have extended BIEM to the Navier–Stokes equations by using the Stokeslet as the fundamental solution.[3–5] The non-linear inertial terms are

0271–2091/91/130355–15$07.50

Received 10 January 1989
Revised 10 October 1990

treated explicitly as volume source terms in these formulations. Clearly, as the non-linear terms become significant (as with increasing Reynolds number), the formulations in References 3–5 can become numerically unstable. For instance, Bush and Tanner[4] were unable to get convergence for flow in a converging channel when the Reynolds numbers were greater than 34. In an alternative formulation Lean and Domoto[6] proposed a novel numerical scheme to solve the 2D incompressible Navier–Stokes equations using BIEM coupled with the method of characteristics (MOC). In the BIEM–MOC approach the vorticity transport equation is modelled as a modified Helmholtz equation with the wave number treated as a function of the flow Reynolds number. The fundamental solution of the BIEM–MOC scheme therefore reflects the Reynolds number dependence of the equations. It can be shown that as the Reynolds number tends to zero, the fundamental solution of the BIEM–MOC scheme is equivalent to the Stokeslet. The non-linear inertial terms in the BIEM–MOC scheme partly manifest themselves as volume vorticity sources. These vorticity sources are computed on a volume grid using trajectory tracking based on the method of characteristics. The present work employs the BIEM–MOC scheme.

Flow in the annulus of cylinders with one or both cylinders rotating has been studied for a number of years. Much of the interest stems from its applications to lubrication technology and bearing design. From a theoretical point of view too this problem is of interest because the flow undergoes separation when the cylinders are sufficiently eccentric, and also because the flow is strongly dependent on the Reynolds number (*Re*). Exact analytical solutions are available for Stokes flow.[7] The effect of inertia at low Reynolds number has been studied using perturbation theory, where the zero-order solution corresponds to Stokes flow.[7,8] Sood and Elrod[9] considered rotation of both inner and outer cylinders and obtained solutions of the complete Navier–Stokes equations using finite difference methods. Recently some numerical solutions for finite Reynolds numbers were presented by San Andres and Szeri[10] using a Galerkin procedure and by Korczak and Patera[11] using spectral methods. Unfortunately none of the above-mentioned studies can be regarded as numerical benchmarks for this problem.

The objective of this paper is to demonstrate the efficacy of integral formulations, such as the BIEM–MOC scheme, for fluid mechanics problems. Flow in the annulus of eccentric cylinders is an attractive test problem because both the geometry and flow characteristics are sufficiently complicated. Solutions are presented for the case where the inner cylinder is rotating and the outer one is fixed. It should be pointed out that, in reality, two-dimensional flows for this case exist only for small rotation rates (low *Re*) because of the appearance of Taylor vortices along the axis for larger rotation rates. Nevertheless, two-dimensional solutions for large *Re* are an interesting computational exercise which can be used to evaluate the performance of numerical schemes. The organization of this paper is as follows. First the BIEM–MOC formulation is presented. Validation of the numerical scheme is achieved by considering the flow in a converging channel (Hamel flow) and comparing with analytical solutions. Next the application of the BIEM–MOC scheme to flow in the annulus of eccentric cylinders is discussed. Solutions are presented for Stokes flow and for Navier–Stokes flow for different Reynolds numbers and compared against the literature. We observe that the solutions for Stokes flow are in excellent agreement with previous analytical and numerical studies. The solutions for Navier–Stokes flow suggest that the separation phenomena may depend strongly on the Reynolds number.

2. BIEM–MOC FORMULATION

We now present briefly the formulation of the BIEM–MOC scheme. Some details about the implementation of this scheme are also available in Reference 6.

The 2D incompressible Navier–Stokes equations in terms of streamfunction and vorticity (ψ–ω) are

$$\nabla^2\psi = -\omega, \tag{1}$$

$$\nabla^2\omega = Re\,\mathrm{D}\omega/\mathrm{D}t, \tag{2}$$

where Re is the flow Reynolds number and ψ and ω have the usual definitions. The substantive derivative in equation (2) can be expressed using a backward time difference along the flow trajectory (streamline),

$$\frac{\mathrm{D}\omega}{\mathrm{D}t} \approx \frac{\omega-\omega_0}{\Delta t} \quad \text{along } \psi = \text{constant},$$

and equation (2) can be rewritten in the form of a *modified Helmholtz equation*,

$$\nabla^2\omega - k^2\omega = -k^2\omega_0, \tag{3}$$

where $k=\sqrt{(Re/\Delta t)}$ is the characteristic wave number.

Integral formulations for equations (1) and (3) can be constructed using standard techniques (see e.g. Reference 12). The integral equations are expressed in terms of the free space Green function for the Laplace equation (G) and the Helmholtz equation (L). Domain integrals involving ω are transformed into boundary integrals. The resulting boundary integral representation of equations (1) and (3) in a region $\mathscr{V}$ enclosed by boundary $\mathscr{S}$ is

$$\gamma\psi(\mathbf{r}) = \int_{\mathscr{S}'}\left(\psi(\mathbf{r}')\frac{\partial G}{\partial n'} - G\frac{\partial\psi(\mathbf{r}')}{\partial n'}\right)\mathrm{d}\mathscr{S}' + \frac{1}{k^2}\int_{\mathscr{S}'}\left(\omega(\mathbf{r}')\frac{\partial H}{\partial n'} - H\frac{\partial\omega(\mathbf{r}')}{\partial n'}\right)\mathrm{d}\mathscr{S}' + \frac{1}{k^2}\int_{\mathscr{V}'} H f\,\mathrm{d}\mathscr{V}', \tag{4}$$

$$\gamma\omega(\mathbf{r}) = \int_{\mathscr{S}'}\left(\omega(\mathbf{r}')\frac{\partial L}{\partial n'} - L\frac{\partial\omega(\mathbf{r}')}{\partial n'}\right)\mathrm{d}\mathscr{S}' + \int_{\mathscr{V}'} L f\,\mathrm{d}\mathscr{V}', \tag{5}$$

where the kernel functions G, L and H are defined as follows:

$$G=(1/2\pi)\ln(k|\mathbf{r}-\mathbf{r}'|), \qquad L=-(1/2\pi)K_0(k|\mathbf{r}-\mathbf{r}'|), \qquad H=G-L.$$

Here K_0 is the modified Bessel function of the second kind and order zero, $f=-k^2\omega_0$ is treated as the volume vorticity source and γ is a geometric factor which is derived from the Cauchy principal value of the integrals involving the normal derivatives of the kernel functions:

$$\gamma = \begin{cases} 0, & \mathbf{r} \ni \mathscr{V}+\mathscr{S}, \\ 1, & \mathbf{r}\in\mathscr{V}, \\ \alpha/2\pi & \mathbf{r}\in\mathscr{S}, \end{cases}$$

where α is the internal angle on the boundary.

Equations (4) and (5) when enforced on discrete elements on the boundary ($\mathbf{r}\in\mathscr{S}$), using either a collocation or Galerkin procedure, result in a set of linear equations of the form

$$\mathbf{A}\omega + \mathbf{B}\omega' + \mathbf{C}\psi + \mathbf{D}\psi' = \mathbf{P}\mathbf{f}, \tag{6}$$

$$\mathbf{E}\omega + \mathbf{F}\omega' = \mathbf{Q}\mathbf{f}, \tag{7}$$

where **A**, **B**, **C**, **D**, **E** and **F** are matrices generated from the integration of the kernels and their normal derivatives over the boundary elements, **P** and **Q** are matrices generated through volume integration of the kernels **H** and **L** respectively, ω, ψ, ω' and ψ' represent column vectors containing values of ω, ψ, $\partial\omega/\partial n$ and $\partial\psi/\partial n$ at the boundary nodes respectively and **f** represents a

column vector of values of f at the volume nodes. Equations (6) and (7) may be solved for ω and ω' provided ψ, ψ' or some linear combination of ψ and ψ' are known on $\mathscr{S}$. Clearly a major advantage of such integral formulations is that vorticity boundary conditions need not be specified *a priori* but can be computed directly as part of the solution.

The velocity field (**v**) in $\mathscr{V}$ can be computed directly by differentiating equation (4). The vorticity distribution in $\mathscr{V}$ can be obtained from equation (5). Since the RHS of equation (6) and (7) depend on ω_0, an iteration is performed by successively updating the values of ω_0 until convergence is attained.

The method of characteristics (MOC) is used to compute ω_0 from ω and **v**. ω_0 is the value of ω one Δt backward in time along trajectories defined by **v** (see Figure 1). Volume discretization is required for the MOC calculation. Quadrilateral elements are used and ω_0 is computed from nodal ω-values using bilinear interpolation. Underrelaxation is often required for convergence:

$$\omega_0^{k+1} = \omega_0^k + \Omega(\omega_0^* - \omega_0^k),$$

where $\Omega < 1$ is the relaxation factor, ω_0^* is the value of ω_0 prior to relaxation and k is the iteration level.

The boundary grid in Helmholtz equation solvers is usually dependent on the wave number. In practice the grid dimension is chosen to be a small fraction of the wavelength.[13] In the context of Navier–Stokes equations and the BIEM–MOC scheme this implies that fine boundary grids are required for large-Reynods-number flows. In addition, fine MOC (volume) grids are required to resolve boundary layer phenomena. Accuracy in the MOC calculation can be preserved by choosing the time step (Δt) to be such that the trajectory moves no more than one volume grid spacing over Δt.

Efficient calculation of ω and **v** in $\mathscr{V}$ at each iteration level is achieved by precomputing the influence coefficient matrices (ICMs). The new values of ω and **v** are computed rapidly by summing the product of the ICMs with the most recent boundary and source distributions. Surface and volume integrals involving singular kernels are evaluated using special schemes which exploit the analytical behaviour of the singular kernels. Details of these integration schemes are discussed elsewhere.[14]

Stokes flow ($Re = 0$) needs to be treated in a special way because the kernel functions G and L become singular as $k \to 0$. The integral equation representation of Stokes flow is

$$\gamma\psi(\mathbf{r}) = \int_{\mathscr{S}'} \left(\psi(\mathbf{r}') \frac{\partial G}{\partial n'} - G \frac{\partial \psi(\mathbf{r}')}{\partial n'} \right) \mathrm{d}\mathscr{S}' - \int_{\mathscr{S}'} \left(\omega(\mathbf{r}') \frac{\partial H}{\partial n'} - H \frac{\partial \omega(\mathbf{r}')}{\partial n'} \right) \mathrm{d}\mathscr{S}', \tag{8}$$

$$\gamma\omega(\mathbf{r}) = \int_{\mathscr{S}'} \left(\omega(\mathbf{r}') \frac{\partial G}{\partial n'} - G \frac{\partial \omega(\mathbf{r}')}{\partial n'} \right) \mathrm{d}\mathscr{S}', \tag{9}$$

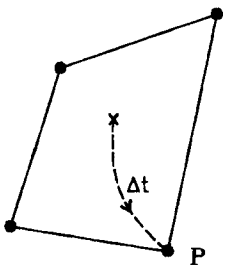

Figure 1. Method of characteristics (MOC) calculation for ω_0 at a volume node. (●, ω, **v** defined; ×, $\omega^P(t-\Delta t)=\omega_0^P$ computed; --- flow trajectory)

where

$$G=(1/2\pi)\ln(|\mathbf{r}-\mathbf{r}'|), \qquad H=(1/8\pi)|\mathbf{r}-\mathbf{r}'|^2(\ln|\mathbf{r}-\mathbf{r}'|-1). \tag{10}$$

Clearly no volume discretization is required for Stokes flow calculations.

Pressure can be recovered from the converged vorticity and streamfunction fields. The pressure gradients in $\mathscr{V}$ can be expressed as

$$\partial P/\partial x = -\partial\omega/\partial y + Re v\omega, \tag{11}$$

$$\partial P/\partial y = \partial\omega/\partial x - Re u\omega, \tag{12}$$

where P is the total pressure and u and w are the velocity components in x and y respectively. From equations (11) and (12) a Poisson equation for pressure can be written as

$$\nabla^2 P = S_P, \tag{13}$$

where the source term S_P is $Re(v\partial\omega/\partial x - u\partial\omega/\partial y + \omega^2)$. The pressure may be evaluated either by integration of equations (11) and (12) along a specified path or through the direct solution of equation (13). Since the former method may give different results depending on the integration path chosen, the latter is preferred. The boundary integral formulation for equation (13) can be written as

$$\gamma P(\mathbf{r}) = \int_{\mathscr{S}'} \left(P(\mathbf{r}')\frac{\partial G}{\partial n'} - G\frac{\partial P(\mathbf{r}')}{\partial n'} \right) \mathrm{d}\mathscr{S}' + \int_{\mathscr{V}'} GS_P \,\mathrm{d}\mathscr{V}'. \tag{14}$$

Pressure along the boundary may be evaluated by integrating the tangential derivative of P, $\partial P/\partial t$, along the boundary, where

$$\partial P/\partial t = -\partial\omega/\partial n + Re\,\omega v_n; \tag{15}$$

t and n represent the tangential and normal directions respectively. Differences may be taken to express $\partial P/\partial t$ in terms of nodal pressure values. Since the BIEM formulation directly solves for ω and $\partial\omega/\partial n$ on the boundary, P on the boundary can be readily determined. Zero pressure can be assumed at some convenient node on the boundary. For multiply connected domains, P can be prescribed on one boundary using the aforementioned procedure, while $\partial P/\partial n$ can be prescribed on the other boundaries using equations (11) and (12).

3. FLOW IN A CONVERGING CHANNEL (HAMEL FLOW)

Hamel flow serves as a useful test problem for validating numerical schemes because exact analytical solutions of the full Navier–Stokes equations exist for comparison. We consider flow between two infinite converging plates with a half-wedge angle of 30°. The computational domain is chosen between an outer radius of 4 and an inner radius of 1/4. This identical test problem has been considered by Gartling *et al.*[15] and also by Bush and Tanner.[4] Analytical solutions to Hamel flow have been discussed by Gartling *et al.* A Stokes velocity profile is assumed at the inlet. $\partial\omega/\partial n$ is set to zero at the outlet, which corresponds to uniform pressure at the outlet. Additionally, purely radial flow is assumed at the inlet and outlet, i.e. $\partial\psi/\partial n = 0$. To exploit the symmetry about the midplane, the kernels G, H and L are appropriately modified. Results discussed here were obtained using 32 boundary elements and 128 volume elements, which is roughly comparable to Grid 1 of Bush and Tanner with 32 boundary elements and 96 volume elements.

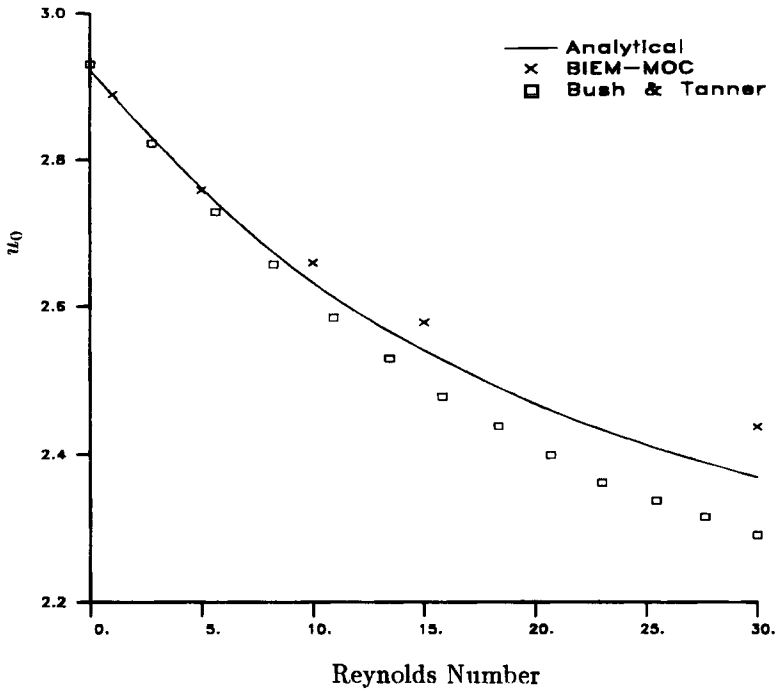

Figure 2. Hamel flow: centreline velocity u_0 at $r=1$ versus Reynolds number

Figure 2 shows a plot of the centreline velocity at $r=1$ as a function of the Reynolds number. Results from the BIEM–MOC scheme and the integral equation approach of Bush and Tanner are compared against the analytical solution. The accuracy of the BIEM–MOC scheme appears comparable to Bush and Tanner. We observe that the accuracy of the solution deteriorates with increasing Reynolds number. This may be a consequence of the coarse mesh as well as the Stokes velocity profile assumed at the inlet. One important result is that the BIEM–MOC scheme converges even for Reynolds numbers of 100 and above whereas Bush and Tanner report loss of convergence for Reynolds numbers above 34. We recall that the Bush and Tanner approach is based on using the Stokeslet as the fundamental solution and attribute the improved convergence in the BIEM–MOC scheme to the fact that its fundamental solution is dependent on the flow Reynolds number.

4. APPLICATION OF BIEM–MOC SCHEME TO FLOW IN ECCENTRIC CYLINDER ANNULUS

The problem geometry together with a typical MOC grid is sketched in Figure 3. The inner cylinder, radius r_1, is rotating counterclockwise with angular velocity Ω_1. The outer cylinder, radius $r_2=2r_1$, is at rest. We assume that the axes of the cylinders are separated by distance e along the x-axis and define the eccentricity as $\varepsilon=e/(r_2-r_1)$. The Reynolds number Re is defined as $Re=Vr_2/v$, where v is the kinematic viscosity of the fluid and $V=\Omega_1 r_1$ is the reference velocity. All lengths are made dimensionless with respect to r_2.

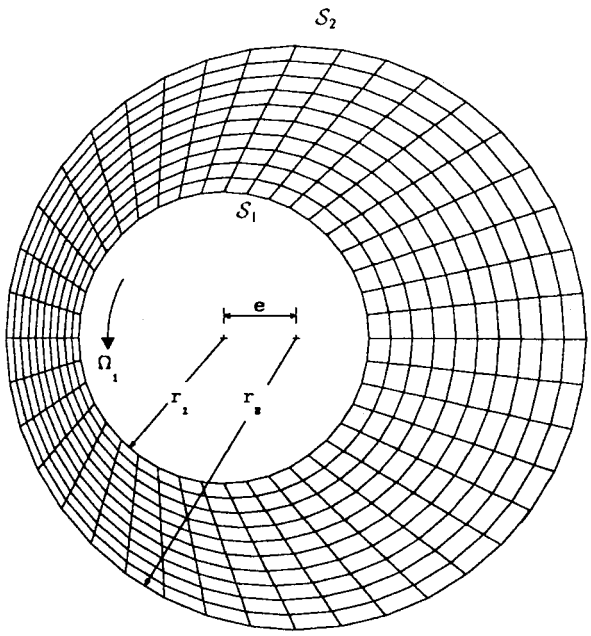

Figure 3. Problem geometry and a typical volume grid for the MOC calculation

The boundary conditions on the inner cylinder ($\mathscr{S}=\mathscr{S}_1$) and the outer cylinder ($\mathscr{S}=\mathscr{S}_2$) are specified as

$$\psi=0, \quad \partial\psi/\partial n=0 \quad \text{on } \mathscr{S}=\mathscr{S}_2, \qquad \partial\psi/\partial n=1 \quad \text{on } \mathscr{S}=\mathscr{S}_1.$$

The value of ψ on $\mathscr{S}_1$, ψ_1, is not known *a priori* and needs to be extracted from the solution. The additional equation needed to compute ψ_1 is obtained by enforcing continuity of pressure on the inner cylinder:

$$\oint_{\mathscr{S}_1} \nabla P \cdot \mathbf{t}\, \mathrm{d}\mathscr{S}=0, \tag{16}$$

where $\mathbf{t}$ is the tangential vector. Substituting for $\nabla P \cdot \mathbf{t}$ from equation (15) and setting v_n equal to zero on a solid boundary, equation (15) can be rewritten as

$$\oint_{\mathscr{S}_1} \frac{\partial\omega}{\partial n}\, \mathrm{d}\mathscr{S}=0. \tag{17}$$

For N boundary nodes on the inner and outer cylinders, equations (6), (7) and (17) give a set of $2N+1$ equations to solve for ω, ω' and ψ_1. For Navier–Stokes flow the computations are repeated until ω_0 converges to a specified tolerance.

Two sets of results are presented here:

(1) Stokes flow, $0 \leq \varepsilon \leq 0{\cdot}9$
(2) Navier–Stokes flow, $\varepsilon=0$, $0{\cdot}5$ and $0 < Re \leq 1000$.

A uniform 80-node boundary mesh (40 on each cylinder) was used for the BIEM computation and a 400-element volume mesh (see Figure 3) was used for the MOC computation. For the concentric cylinder case, 40 boundary elements and 100 volume elements were used. The system

matrix was generated using collocation, i.e. the boundary conditions were explicitly enforced on each element. All computations were carried out on an IBM 3090-600E computer using the vector facility. The CPU time for Stokes flow computations was approximately 3 s. The Navier–Stokes flow for the eccentric cylinder cases required approximately 180 s for pre-computing the ICM matrices and about 1 s per iteration for the transient computation.

4.1. *Stokes flow*

The purpose of the Stokes flow computations was to calibrate the algorithm by comparing with exact analytical results. Table I tabulates ψ_1 and the angle of separation (θ_s) using zero-order elements and linear elements and also provides comparisons with analytical predictions. The analytical expressions were first given by Kamal[7] and later corrected by Kelmanson.[2] Flow separation occurs between $\varepsilon = 0{\cdot}3$ and $0{\cdot}4$.

An interesting observation for Stokes flow in this geometry is the existence of a Γ-contour at $r = 1$.[16] Γ-contours are mathematical artefacts which appear as a result of the logarithmic nature of kernel G. To elaborate this point, consider the case of concentric cylinders ($\varepsilon = 0$). The integral $I_1 = \int_{\mathscr{S}'} G(\partial\psi/\partial n')\,\mathrm{d}\mathscr{S}'$ appearing in equation (8) can be written as

$$I_1 = \left(\frac{\partial\psi}{\partial n}\right)_{\mathscr{S}_1} \int_{\mathscr{S}_1} G\,\mathrm{d}\mathscr{S} + \left(\frac{\partial\psi}{\partial n}\right)_{\mathscr{S}_2} \int_{\mathscr{S}_2} G\,\mathrm{d}\mathscr{S},$$

since $\partial\psi/\partial n$ is constant on $\mathscr{S}_1$ and $\mathscr{S}_2$. Evaluating the integrals in the above expression, we obtain

$$I_1(r) = \left(\frac{\partial\psi}{\partial n}\right)_{\mathscr{S}_1} \ln r + \left(\frac{\partial\psi}{\partial n}\right)_{\mathscr{S}_2} \ln r_2.$$

Clearly, when $r_2 = 1$, I_1 is independent of $(\partial\psi/\partial n)_{\mathscr{S}_2}$ and the resulting solution need not satisfy the boundary condition on $\mathscr{S}_2$. The Γ-contour problem can be easily circumvented by redefining the kernel functions G and H as

$$G = (1/2\pi)\ln(C|\mathbf{r}-\mathbf{r}'|), \qquad H = (1/8\pi)|\mathbf{r}-\mathbf{r}'|^2[\ln(C|\mathbf{r}-\mathbf{r}'|)-1],$$

where $C \neq 1$ is any positive constant. This modification of G and H amounts to rescaling the lengths in the problem to avoid a vanishing kernel at unit radius. Results in Table I have been

Table I. Stokes flow: comparison of numerical and analytical results

ε	Zero-order elements			Linear elements			Analytical	
	ψ_1	θ_s(deg)	Error*	ψ_1	θ_s(deg)	Error*	ψ_1	θ_s(deg)
0	0·2122		$0{\cdot}8\times10^{-12}$	0·2113		$0{\cdot}2\times10^{-12}$	0·2121	
0·1	0·2094		$0{\cdot}7\times10^{-8}$	0·2085		$0{\cdot}1\times10^{-7}$	0·2093	
0·2	0·2011		$0{\cdot}1\times10^{-7}$	0·2002		$0{\cdot}2\times10^{-7}$	0·2010	
0·3	0·1876		$0{\cdot}1\times10^{-7}$	0·1868		$0{\cdot}3\times10^{-7}$	0·1876	
0·4	0·1695	−65·6	$0{\cdot}2\times10^{-7}$	0·1687	−66·3	$0{\cdot}3\times10^{-7}$	0·1696	−57·1
0·5	0·1475	−95·7	$0{\cdot}3\times10^{-7}$	0·1467	−97·3	$0{\cdot}4\times10^{-7}$	0·1476	−83·1
0·6	0·1222	−116·0	$0{\cdot}2\times10^{-6}$	0·1214	−117·9	$0{\cdot}2\times10^{-6}$	0·1223	−102·8
0·7	0·0944	−132·3	$0{\cdot}6\times10^{-5}$	0·0935	−133·5	$0{\cdot}1\times10^{-4}$	0·0944	−120·2
0·8	0·0648	−146·3	$0{\cdot}3\times10^{-2}$	0·0632	−146·1	$0{\cdot}3\times10^{-2}$	0·0644	−136·9
0·9	0·0330	−159·0	$0{\cdot}3\times10^{-1}$	0·0332	−158·0	$0{\cdot}3\times10^{-1}$	0·0328	−154·1

* Error $= |\int_{\mathscr{S}_2} (\partial\omega/\partial n)\,\mathrm{d}\mathscr{S}|$ is the error in satisfying pressure continuity on the outer cylinder.

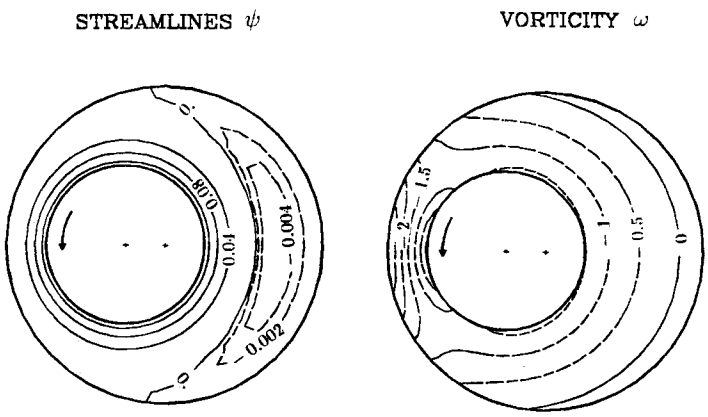

Figure 4. Streamfunction (ψ) and vorticity (ω) contours for Stokes flow ($\varepsilon = 0{\cdot}5$)

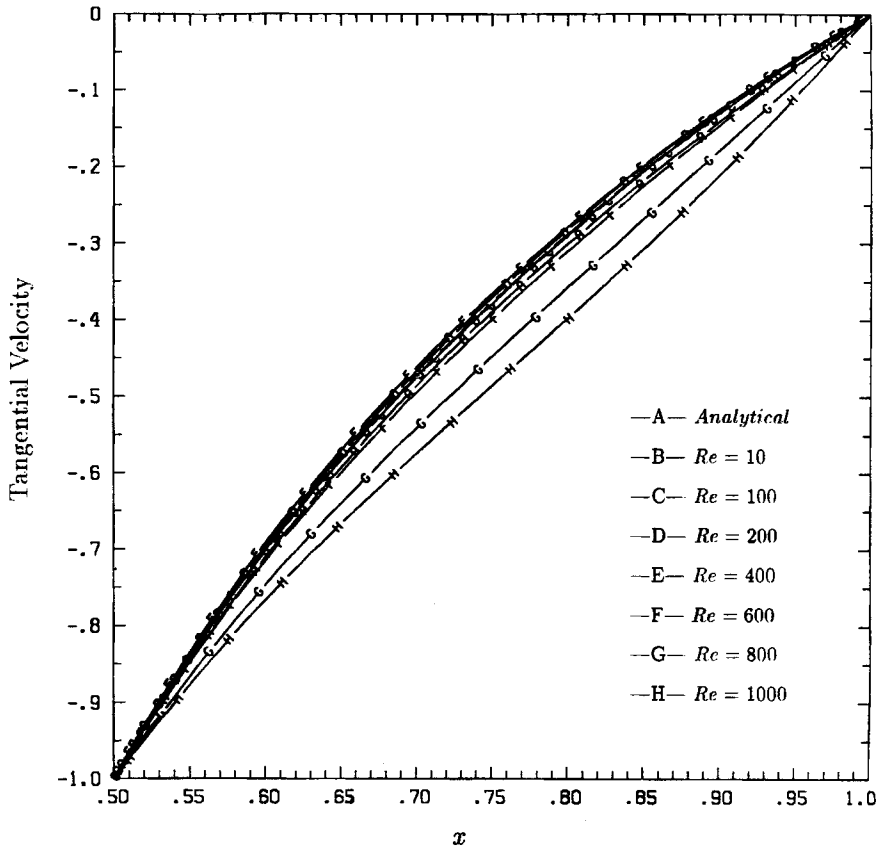

Figure 5. Tangential velocity in the annulus of concentric cylinders ($\varepsilon = 0$)

obtained using $C=1{\cdot}1$ for $\varepsilon \leq 0{\cdot}8$ and $C=2$ for $\varepsilon=0{\cdot}9$. For large ε it is observed that better precision can be obtained by using larger values of C.

The values of ψ_1 are in excellent agreement with analytical results. The separation and reattachment points are the points on the outer cylinder where ω vanishes. The separation angles are observed to be consistently higher than the analytical predictions. Kelmanson[2] also observed higher values of θ_s with a maximum discrepancy of 8°, even with 160 boundary nodes. This discrepancy in the value of θ_s is not entirely surprising because the largest errors in boundary integral formulations occur near the boundary. Linear elements do not appear to be more accurate than zero-order elements. For large ε the error in satisfying the pressure periodicity condition on the outer cylinder is quite significant, which indicates the need for a finer boundary mesh. In Figure 4 the streamfunction and vorticity contours are plotted for $\varepsilon=0{\cdot}5$. As expected, these contours are exactly symmetric about the x-axis.

4.2. Navier–Stokes flow

We first consider the trivial case of concentric cylinders ($\varepsilon=0$). For this case the flow solution is independent of the Reynolds number. Figure 5 displays the tangential velocity profile in the annulus as a function of the Reynolds number. Considerable departure from the analytical solution can be clearly observed for Reynolds numbers greater than 600.

Table II summarizes the Navier–Stokes computations for the eccentric cylinder cases ($\varepsilon=0{\cdot}5$). A larger number of iterations are required as Re is increased. The iteration count can be

Table II. Navier–Stokes flow: summary of computer simulations for $\varepsilon=0{\cdot}5$, $\Delta t=0{\cdot}025$

Re	Initial ω_0	Ω	Exit* (%)	Error†	Iterations
1	$-2/3$	0·6	0·2	$7{\cdot}5\times10^{-4}$	100
10	$Re=1$	0·5	0·2	$4{\cdot}3\times10^{-4}$	100
50	$Re=1$	0·4	0·1	$1{\cdot}2\times10^{-4}$	200
100	$Re=50$	0·35	0·1	$1{\cdot}3\times10^{-4}$	164
200	$Re=100$	0·3	0·2	$9{\cdot}5\times10^{-4}$	250
300	$Re=200$	0·25	0·2	$1{\cdot}5\times10^{-3}$	250
400	$Re=300$	0·2	0·16	$2{\cdot}1\times10^{-3}$	250
500	$Re=400$	0·15	0·12	$2{\cdot}7\times10^{-3}$	250

* Exit $=\max|(\omega_0^{(k+1)}-\omega_0^{(k)})/\omega_0^{(k)}|$ is the convergence criterion.
† Error $=|(1/k^2)\int_{\mathscr{S}_2}(\partial\omega/\partial n)\,\mathrm{d}\mathscr{S}|$ is the error in satisfying pressure continuity on the outer cylinder.

Table III. Navier–Stokes flow: ψ_1, θ_s and θ_r versus Re for $\varepsilon=0{\cdot}5$, $\Delta t=0{\cdot}025$

Re	ψ_1	θ_s(deg)	θ_r(deg)
1	0·1475	−96·2	96·2
10	0·1478	−94·7	94·6
50	0·1474	−91·8	91·0
100	0·1452	−95·6	93·7
200	0·1356	−109·2	108·4
300	0·1203	−122·5	124·9
400	0·1004	−136·7	141·4
500	0·0779		

optimized by using converged results from previous runs as initial guesses for ω_0. As Re is increased, the non-linear advection terms in the Navier–Stokes equations become significant and the evaluation of ω_0 becomes critical. Accurate evaluation of ω_0 is often difficult in regions of sharp gradients such as boundary layers. The error term in Table II signifies the extent to which pressure periodicity is satisfied on the outer cylinder. Although the pressure periodicity condition is not explicitly enforced on the outer cylinder, it must still be satisfied by the converged solution. The observed discrepancies are primarily due to accumulated errors in the ω_0 calculation during

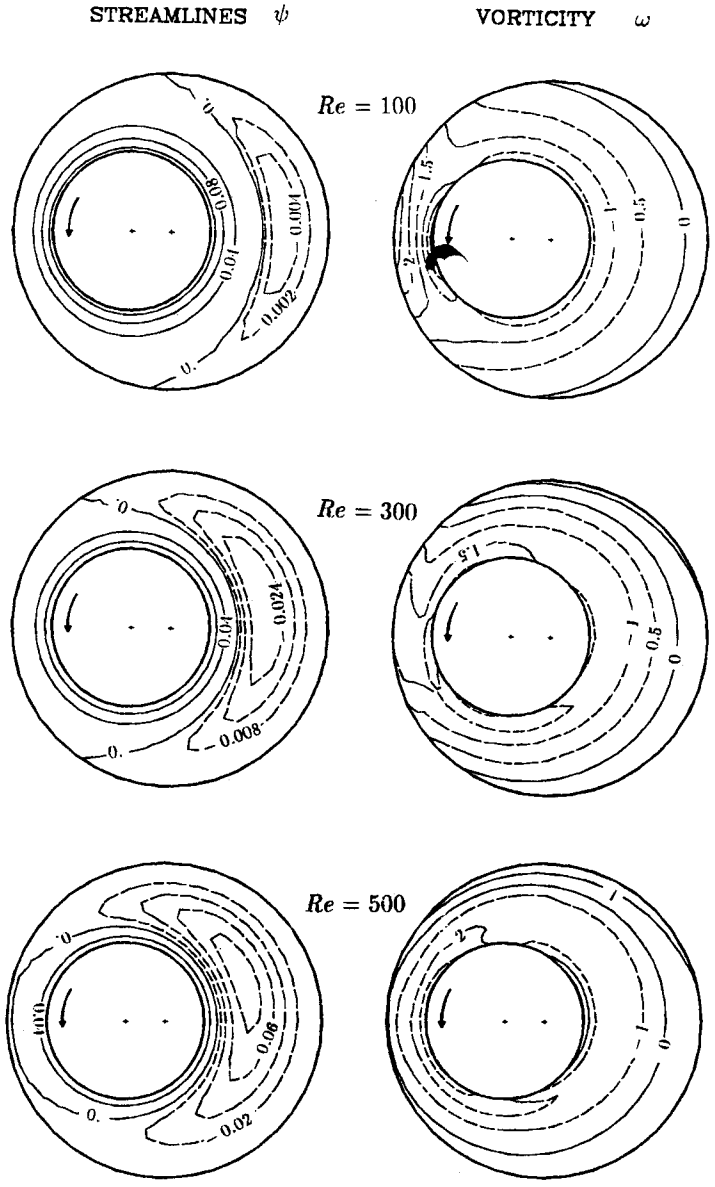

Figure 6. Streamfunction (ψ) and vorticity (ω) contours for Navier–Stokes flow

the MOC procedure. These errors may be reduced by using a finer volume mesh or a spatially graded mesh.

Table III gives the values of ψ_1, the separation angle (θ_s) and the reattachment angle (θ_r) as a function of *Re*. The solution for $Re=1$ is consistent with the Stokes flow solution for $\varepsilon=0{\cdot}5$. ψ_1 is the volume flow rate between the inner cylinder and the separation streamline. We find that ψ_1 decreases consistently with *Re* for $Re>100$. These appears to be some controversy in the literature regarding the effect of inertia on the separation and reattachment points. The perturbation analysis of Kamal[7] suggests that the effect of inertia is to move the point of separation against the direction of Ω_1 and the point of reattachment in the direction of Ω_1, which is supported by Sood and Elrod[9] as well. However, results of San Andres and Szeri[10] suggest that the separation point moves in the direction of Ω_1 whereas the reattachment point moves against the direction of Ω_1 as *Re* is increased. Our results agree with San Andres and Szeri for low *Re* ($Re<50$) and with Kamal for higher *Re*. For $Re=500$, ω is greater than zero everywhere on the outer cylinder, which indicates that both points of separation and reattachment are within one boundary element.

The vorticity and streamlines contours as a function of *Re* are plotted in Figure 6. The centre of the separation eddy moves in the direction of rotation, which is consistent with the literature.[9-11] The ψ-value at the centre of the separation eddy increases with *Re* because of the stronger recirculation.

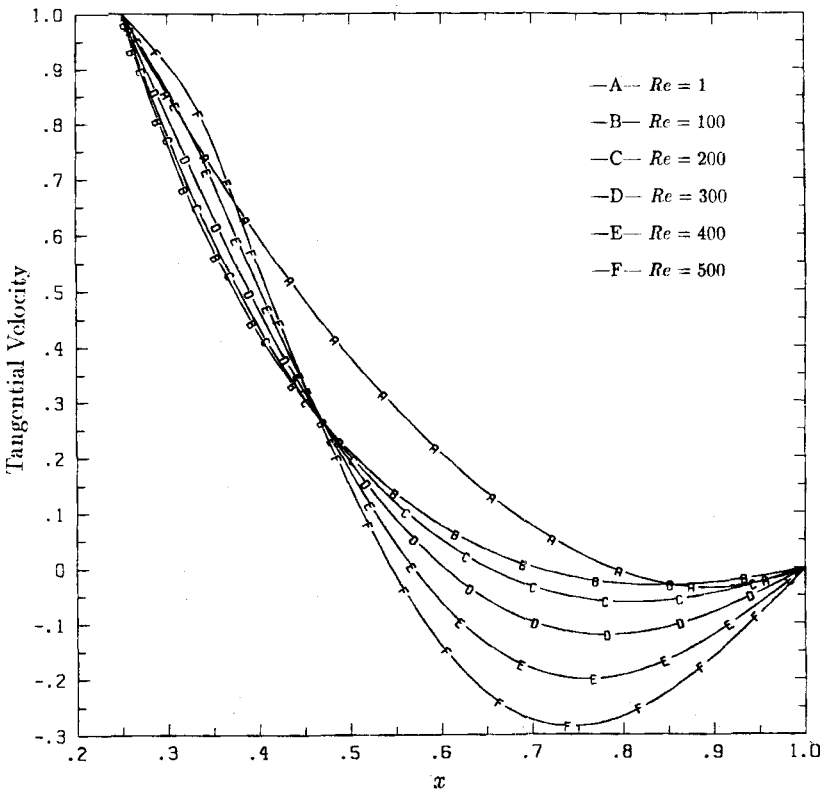

Figure 7. Tangential velocity distribution at the narrow gap for $\varepsilon=0{\cdot}5$

The tangential velocity profiles at the narrow gap ($\theta=180°$) and the wide gap ($\theta=0°$) are shown in Figures 7 and 8 respectively. In the narrow gap the tangential velocity gradient ($\partial v_t/\partial n$) on the outer cylinder approaches zero as Re is increased to 500. Since $\partial v_t/\partial n=0$ on the solid boundary implies zero vorticity, it appears as though both the points of separation and reattachment for $Re=500$ are at $\theta_s=\theta_r=180°$. The tangential velocity profile in the wide gap (Figure 8) indicates an increased region of separation (negative velocities) as well as higher velocities in the separation eddy at higher Reynolds numbers. The shapes of the tangential velocity profiles for low Re are consistent with Sood and Elrod.[9]

The effect of inertia on the static pressure distribution is shown in Figure 9. Zero pressure is assumed at $\theta=180°$ on the inner cylinder. For Stokes flow ($Re=0$) the pressure contours are exactly antisymmetric about the x-axis, with the region of positive pressure above and the region of negative pressure below. Upon inclusion of inertial effects the antisymmetric behaviour disappears and an increased region of positive pressure is observed. For $Re=10$ the region of positive pressure can be observed extending below the x-axis. For $Re=50$ and 100 the region of negative pressure shrinks even further and appears to be localized around the inner cylinder, while positive pressure exists everywhere else.

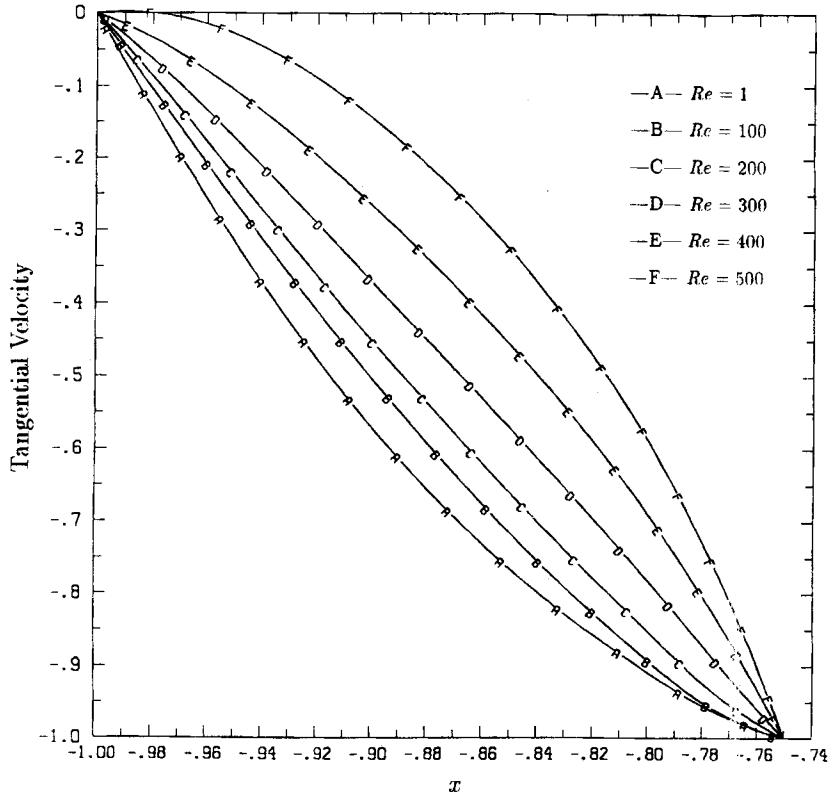

Figure 8. Tangential velocity distribution at the wide gap for $\varepsilon=0{\cdot}5$

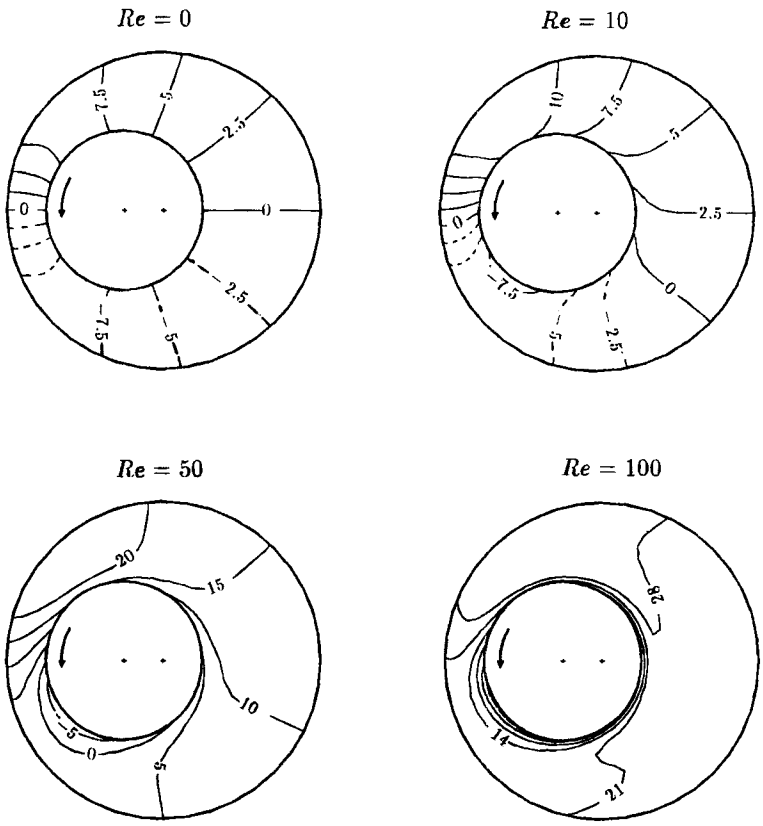

Figure 9. Effect of inertia on the pressure distribution in the cylinder annulus

5. CONCLUDING REMARKS

A novel Navier–Stokes solver based on boundary integral methods is discussed here. This method differs from past attempts to use integral equation methods on Navier–Stokes equations in that the fundamental solution depends on the flow Reynolds number and consequently has better stability at high Reynolds numbers. The scheme offers the traditional advantages of boundary integral methods such as reduced problem size and ability to handle arbitrarily shaped 2D geometries including multiply connected regions. Another key advantage is being able to zoom into the problem domain and obtain high-resolution field data during post-processing without needing to recompute the solution.

We foresee two areas of improvement to the BIEM–MOC scheme. The first involves improving the accuracy of the MOC procedure. In the solution of purely advective flows using the method of characteristics it is now known that evaluating the dependent parameter along the trajectory using a bilinear interpolation of the four surrounding nodal values introduces excessive numerical damping. This damping can be eliminated by using higher-order interpolations (such as Hermite bicubic[17]) which are constructed from the nodal values of the dependent parameter and their derivatives. The current implementation of the BIEM–MOC scheme uses a bilinear interpolation in the MOC procedure, and this will be inadequate at high Reynolds numbers when advection dominates. The second area of improvement relates to the rate of convergence of the

iterative procedure. A combination of Newton–Raphson and relaxation schemes may provide a faster rate of convergence. In its present form the BIEM–MOC scheme appears to provide good accurate solutions for low Reynolds number and stable but less accurate solutions at higher Reynolds numbers. The use of influence coefficient matrices (ICMs) provides a way to rapidly compute boundary and volume fields during iterations. Further enhancements in speed are possible with the use of parallel processing. Natural extensions to the present work could involve extending the scheme to primitive variables and to 3D geometries.

ACKNOWLEDGEMENTS

The computational support for this work was provided by the Cornell National Supercomputer Facility, a resource of the Center for Theory and Simulation in Science and Engineering (Cornell Theory Center), which receives major funding from the National Science Foundation and IBM Corporation in addition to support from New York State and members of the Corporate Research Institute.

REFERENCES

1. M. A. Jawson, 'Integral equation methods in potential theory I', *Proc. R. Soc. A*, **273**, 237–246 (1963).
2. M. A. Kelmanson, 'A boundary integral equation method for the study of slow flow in bearings with arbitrary geometries', *J. Tribol.*, **106**, 260–264 (1984).
3. P. Skerget, A. Alujevic and C. A. Brebbia, 'Analysis of laminar fluid flows by boundary elements', *Proc. 4th Int. Conf. on Numerical Methods in Laminar and Turbulent Flow, Vol. 1*, C. Taylor (ed.), Pineridge Press, Swansea, U.K., 1985, pp. 22–38.
4. M. B. Bush and R. I. Tanner, 'Numerical solution of viscous flows using integral equation methods', *Int. j. numer. methods fluids*, **3**, 71–92 (1983).
5. N. Tosaka and K. Onishi, 'Boundary integral equation formulations for steady Navier–Stokes equations using Stokes fundamental solutions', *Eng. Anal.*, **2**, 128–132 (1985).
6. M. H. Lean and G. A. Domoto, 'Charge transport in Navier–Stokes flow', *IEEE Trans. Magnetics*, **MAG-24**, 262–265 (1988).
7. M. M. Kamal, 'Separation in the flow between eccentric rotating cylinders', *J. Basic Eng. D*, **88**, 717–724 (1966).
8. B. Y. Ballal and R. S. Rivlin, 'Flow of Newtonian fluid between eccentric rotating cylinders: inertia effects', *Arch. Rat. Mech. Anal.*, **62**, 237–294 (1977).
9. D. R. Sood and H. G. Elrod, 'On the flow between two long eccentric cylinders', *Report No. 17*, Lubrication Research Laboratory, Department of Mechanical Engineering, Columbia University, 1970.
10. A. San Andres and A. Z. Szeri, 'Flow between eccentric rotating cylinders', *J. Appl. Mech.*, **51**, 869–878 (1984).
11. K. Z. Korczak and A. T. Patera, 'An isoparametric spectral element method for solution of the Navier–Stokes equations in complex geometry', *J. Comput. Phys.*, **62**, 361–382 (1986).
12. J. A. Liggett and P. L.-F. Liu, *The Boundary Integral Equation Method for Porous Media Flow*, George Allen and Unwin, London, 1983.
13. G. J. Burke and A. J. Poggio, 'Numerical electromagnetic code (NEC)—method of moments, Parts I & II', *Tech. Doc. # 116*, Naval Ocean Systems Center, 1977.
14. P. S. Ramesh and M. H. Lean, 'Accurate integration of singular kernels in boundary integral formulations for Helmholtz equations', *Int. j. numer. methods eng.*, (1991).
15. D. K. Gartling, R. E. Nickell and R. I. Tanner, 'A finite element convergence study for accelerating flow problems', *Int. j. numer. methods eng.*, **11**, 1155–1174 (1977).
16. P. L.-F. Liu and M. H. Lean, 'A note on Γ-contours in the integral equation formulation for a multiply-connected region', *BETECH 90, 5th Int. Conf. on Boundary Element Technology*, University of Delaware, 10–12 July 1990.
17. F. M. Holly Jr. and J. Usseglio-Polatera, 'Dispersion simulation in two-dimensional tidal flow', *J. Hydraul. Div., Proc. ASCE*, **110**, 905–926 (1984).